



ARTICLE

Synthesis, characterization, biological activity, and corrosion inhibition in acid medium of unsymmetrical tetradentate N_2O_2 Schiff base complexes

Amani S. Alturiqi¹ | Abdel-Nasser M.A. Alaghaz^{2,3} | Mohamed E. Zayed⁴ | Reda A. Ammar^{5,6}

¹Department of Chemistry, College of Science, Princess Nourah bint Abdul Rahman University, Riyadh, Saudi Arabia

²Department of Chemistry, Faculty of Science, Jazan University, Jazan, Saudi Arabia

³Department of Chemistry, Faculty of Science (Boys), Al-Azhar University, Cairo, Egypt

⁴Department of Botany and Microbiology, Faculty of Science, King Saud University, Riyadh, Saudi Arabia

⁵Department of Chemistry, College of Science, Al-Imam Mohammad Ibn Saud Islamic University (IMSIU), Riyadh, Saudi Arabia

⁶Department of Chemistry, Faculty of Science (Girls), Al-Azhar University, Cairo, Egypt

Correspondence

Abdel-Nasser M.A. Alaghaz, Department of Chemistry, Faculty of Science, Jazan University, Jazan, Saudi Arabia.
Email: aalaghaz@hotmail.com

Funding information

Deanship of Scientific Research at Princess Nourah bint Abdulrahman University, Grant/Award Number: RGP-1438-00

Four divalent metal(II) complexes, namely $[Co(II)L(H_2O)Cl] \cdot 2H_2O$, $[Ni(II)L(H_2O)Cl] \cdot 4H_2O$, $[Cu(II)L(H_2O)Cl] \cdot 3H_2O$, and $[Zn(II)L(H_2O)Cl] \cdot 5H_2O$, $\{L = 2\text{-furan-2-ylmethyleneamino-phenyl-iminomethylphenol}\}$, were synthesized and characterized by several techniques. The molar conductance measurement of all analyzed complexes in DMSO showed their non-electrolytic nature. The new Schiff base ligand (HL) acts as tetradentate ligand, coordinated through deprotonated phenolic oxygen, furan ring oxygen, and two azomethine nitrogen atoms. The ligand field parameters were measured for the metal complexes, which were found to be in the range notified for an octahedral structure. The molecular structural parameters of the synthesized HL ligand and its related metal(II) complexes were calculated and correlated with the experimental parameters such as infrared (IR) data. The investigated ligand and metal complexes were screened for their in vitro antimicrobial activities against different types of fungal and bacterial strains. The resulting data confirmed the examined compounds as a highly promising bactericides and fungicides. The antitumor activities of all inspected compounds were evaluated against colon carcinoma (HCT-116) and mouse myelogenous leukemia carcinoma (M-NFS-60) cell lines. The inhibition effect of HL ligand and its isolated complexes on the corrosion carbon in the form of a rod of area 0.35 cm^2 in HCl was investigated by measuring the weight loss at $25 \text{ }^\circ\text{C}$.

KEYWORDS

antimicrobial, antitumor, DFT, furan-Schiff base complex, spectroscopic data

1 | INTRODUCTION

Schiff bases have played a major role in the development of coordination chemistry, and the synthesis of Schiff bases is one of the main activities in the areas of biochemistry, materials science, hydrometallurgy, catalysis, activation, transport and separation phenomena, etc.^[1,2] Unsymmetrical Schiff base ligands with hard and soft atoms have been widely investigated. They readily form stable complexes with most of the transition metals, and the synthesis of these complexes is an important area of study with implications in bioinorganic chemistry,^[3–5] catalysis,^[6] and medicinal chemistry.^[7] Unsymmetrical Schiff base ligands with N, O, and S donors

have been able to provide diverse possibilities in the structure and chemical properties, and these complexes are the most abundant and dominate the field. The presence of both hard and soft donor atoms in one ligand increases the coordination ability toward hard as well as soft metals.^[8–11] The interest in the coordination chemistry of tridentate unsymmetrical Schiff base ligands with NOS donating sites has increased because of their capability of forming stable complexes of four, five, and six coordination^[12,13] and because they show a broad range of antifungal,^[14] antibacterial,^[15] and anticancer properties.^[16] Tridentate NOS donor unsymmetrical Schiff base ligands have been able to form 1:1 and/or 1:2 complexes. In all complexes, the Schiff base

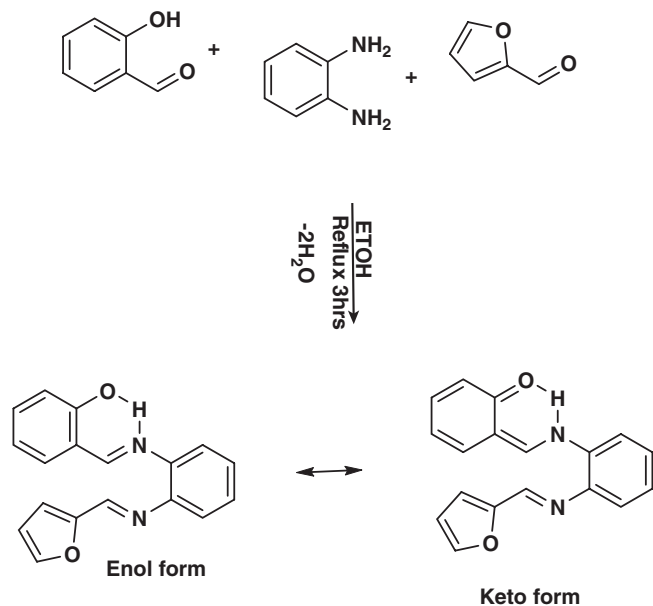


FIGURE 1 Synthesis and proposed structure of the ligand (HL)

ligand behaves as an NOS-tridentate ligand or an NS (with soft metal ions) and/or NO-bidentate (with hard metal ions) ligand. The most plausible geometry for the 1:2 complexes or the 1:1 complexes appears to be square-planar (four-coordinated), trigonal-bipyramidal (five-coordinated), or octahedral (six-coordinated).^[12] In this paper, we describe the synthesis and characterization of Co(II), Ni(II), Cu(II), and Zn(II) complexes with the furan-Schiff base ligand (HL) (Figure 1). The possible geometries for the related furan-Schiff base metal(II) complexes were deduced by elemental analysis, molar conductance, magnetic susceptibility, infrared (IR), electronic and thermal analysis, X-ray diffraction (XRD), electron paramagnetic resonance (EPR), and molecular modeling studies.

2 | EXPERIMENTAL

2.1 | Materials and methods

Elemental analyses (C, H, N) were carried out on a Perkin-Elmer 2,408 CHN analyzer. Electronic spectra were recorded on a UV2 Unicam UV-vis spectrophotometer. Magnetic moments (μ_{eff}) were measured with a Sherwood scientific magnetic susceptibility balance at 294 K. IR spectra were recorded on a Mattson 5000 Fourier transform infrared (FTIR) spectrophotometer. ¹H NMR measurements at room temperature were carried out on a Varian Gemini 200 MHz spectrometer, a Varian-Mercury VX-300 NMR spectrometer, and a Bruker 500 (Avance iii) instrument. Molar conductivities were measured in DMSO solution for the complexes (10^{-3} M) using a CON 6000 conductivity meter (Cyberscan, Eutech instruments). Magnetic susceptibilities of the complexes were calculated by the modified Gouy method at room temperature using a magnetic susceptibility balance (Johnson Matthey, UK). The effective magnetic moments were

calculated using the relation $\mu_{\text{eff}} = 2.828(\chi_{\text{m}}T)^{1/2}$ BM, where χ_{m} is the molar magnetic susceptibility corrected for the diamagnetism of all atoms in the compounds using Selwood and Pascal's constants. Thermal analysis (TG) was effected by using a Shimadzu TG-50 thermal analyzer at the heating rate of 10 °C/min in nitrogen atmosphere at the rate 20 mL/min in the temperature range 30–1100 °C using platinum crucibles. Powder XRD patterns were recorded with an X'Pert PRO diffractometer using Cu K α_1 radiation ($\lambda = 1.54060$ Å) at the operating voltage of 40 kV and current of 30 mA. Thermal studies were conducted using the Q 600SDT and Q 20 DSC thermal analyzers. The biological activity experiments were conducted at the Bab-Al-Sheria University Hospital (Al-Azhar Microbiology Laboratory University).

2.2 | Corrosion test by weight loss measurement

Six parallel steel sheets of dimensions 2.0 × 2.0 × 0.1 cm were abraded with emery paper (grade to 1200 grit size) and then washed with double-distilled water and acetone. After accurate weighing, the specimens were immersed in a 250-mL beaker containing 100 mL of HCl with and without the addition of different concentrations of the ligand and metal complexes. All the aggressive acid solutions were open to air, and the measurements were carried out at room temperature (25 ± 1 °C). After 2 hr, the specimens were taken out, washed, dried, and weighted again accurately. The experiment was repeated, and the average weight loss of the six the parallel steel sheets was obtained. The inhibition efficiency (%IE) of the investigated compounds for the corrosion of steel in HCl was calculated as follows:

$$\%IE = (R_0 - R_i/R_0) \times 100 \quad (1)$$

where R_0 and R_i are the rates of reaction in the absence and presence of the inhibitor, respectively. The experiment was repeated at 2, 4, and 8 hr. The corrosion inhibition of the compounds was tested on carbon in the form of a rod of area 0.35 cm². Steel has the composition (in wt%) 0.18 C, 0.06 Si, and the rest Fe, 0.95 Mn, 0.013 Ni, 0.009 P, 0.004 S, 0.6 Si, 0.008 Cr, 0.033 Al, 0.16 V, 0.004 Ti, and 0.00 Cu. The method of weight loss was used to study the corrosion inhibition of carbon steel at 25 °C.

2.3 | Synthesis of the Schiff base ligand

The new furan-Schiff base ligand (HL) was prepared by adding benzene 1,2-diamine (0.108 g, 1 mmol), 2-hydroxybenzaldehyde (0.122 g, 1 mmol), and furan-2-carbaldehyde (0.096 g, 1 mmol) and dissolving them in dry absolute ethanol (40 mL). The reaction mixture was heated under reflux for 3 hr, and a yellow precipitate was formed upon cooling the solution to room temperature. The product was filtered off and washed with a small quantity of ethanol and then diethyl ether, air-dried, and recrystallized from ethanol. The purity of the prepared furan-Schiff base

TABLE 1 Formula, molecular weight, melting point, yield, and elemental analysis data of the complexes

No.	Compound M.F. (M.W.)	Color	M.P. (°C)	Yield (%)	Elemental analysis calc. (found)					Λ_m^a
					C	H	N	Cl	M	
Ligand	HL C ₁₈ H ₁₄ N ₂ O ₂ (290.3)	Orange	142	93	74.47 (74.68)	4.86 (4.73)	9.65 (9.52)	—	—	—
1	[CoL(H ₂ O)Cl].2H ₂ O C ₁₈ H ₁₉ ClN ₂ O ₅ Co (437.7)	Olive	>300	86	49.39 (49.39)	4.38 (4.38)	6.40 (6.37)	8.10 (8.04)	13.46 (13.42)	7.32
2	[NiL(H ₂ O)Cl].4H ₂ O C ₁₈ H ₂₃ ClN ₂ O ₇ Ni (473.5)	Brown	>300	84	45.66 (45.53)	4.90 (4.88)	5.92 (5.82)	7.49 (7.43)	12.39 (12.34)	9.12
3	[CuL(H ₂ O)Cl].3H ₂ O C ₁₈ H ₂₁ ClN ₂ O ₆ Cu (460.4)	Pale brown	>300	83	46.96 (46.91)	4.60 (4.55)	6.09 (6.02)	7.70 (7.68)	13.80 (13.76)	6.54
4	[ZnL(H ₂ O)Cl].5H ₂ O C ₁₈ H ₂₅ ClN ₂ O ₈ Zn (498.2)	Orange	>300	86	43.39 (43.33)	5.06 (5.00)	5.62 (5.57)	7.12 (7.08)	13.12 (13.09)	8.36

M.P. melting point; M.F. = molecular formula; M.W. = molecular weight.

^a Λ_m = molar conductance ($\Omega^{-1} \text{ cm}^2 \text{ mol}^{-1}$).

ligand was measured by thin-layer chromatography (TLC) employing silica gel, as shown in (Figure 1).

2.4 | Synthesis of the metal(II) Schiff base complexes

The new furan-Schiff base (HL) ligand (1 mmol) was dissolved in 10 mL of dichloromethane, then 1 mmol of CoCl₂·6H₂O, NiCl₂·6H₂O, CuCl₂·2H₂O, or ZnCl₂ dissolved in 10 mL of ethanol was added dropwise, and the reaction mixture was stirred and heated at 50 °C for 4 hr. The solvent was allowed to evaporate slowly to give a solid. The resulting product was collected by filtration and washed with dichloromethane and ethyl acetate to get the pure complex. The physical properties and analytical data of the new furan-Schiff base ligand and its corresponding metal(II) complexes are given in Table 1.

2.5 | Molecular modeling

Calculations using the DMOL³ program were performed in the Materials Studio package,^[17] which is designed for the realization of large-scale density functional theory (DFT) calculations. DFT semi-core pseudo-pods (dsp) calculations were performed with the double numerical basis sets plus polarization functional (DNP). The DNP basis sets are comparable in quality to the 6–31G Gaussian basis sets.^[18] Delley et al. showed that the DNP basis sets are more accurate than Gaussian basis sets of the same size.^[19] The RPBE functional^[20], so far the best exchange-correlation functional,^[21] based on the generalized gradient approximation (GGA), was employed to take into account the exchange and correlation effects of electrons. Geometric optimization was performed without any symmetry restriction.

3 | RESULTS AND DISCUSSION

3.1 | Characterization of the Schiff base ligand (HL)

3.1.1 | Elemental analyses

The novel azomethine furan-Schiff base HL ligand was prepared and subjected to elemental, mass, and IR spectral analyses. Results of the microanalytical data (C, H, N), along with the molecular formula (M.F.) and the melting point (M.P.), are given in Table 1. The results obtained are in good agreement with those calculated for the suggested formula, and the melting point is sharp, indicating the purity of the prepared azomethine furan-Schiff base HL ligand. The structure of the azomethine furan-Schiff base HL ligand under study is shown in Figure 1.

3.1.2 | IR spectrum

The IR spectrum (Table 2) of furan-Schiff base HL ligand is given in “synthetic procedures”. Vibration bands at 3,364 cm⁻¹ (ν O–H), 3,076 cm⁻¹ (ν C–H, Ar–H), 1,623 cm⁻¹ (ν CH=N), 1,567 cm⁻¹ (ν C=C), and 1,214 cm⁻¹ (ν C–O, Ar–O) were observed for the azomethine Schiff base ligand (HL) (Figure S1, Supporting information). The stretching frequency at 2853 cm⁻¹ in the furan-Schiff base HL ligand indicates the presence of the O–H···N intramolecular hydrogen bond. The HL ligand with a strong band at 1,214 cm⁻¹ possesses highest percentage of enolimino tautomer because of the stabilization of the phenolic C–O bond. Similarly, the band at 1,024 cm⁻¹ in the HL ligand corresponds to the ν (C–O–C) stretching vibration of the furan ring.^[22]

TABLE 2 IR spectral data (cm⁻¹) of the furan-Schiff's base HL ligand and its metal complexes

Compound	ν_{OH}	$\nu_{\text{(OH)water}}$	$\nu_{\text{C=N}}$	$\nu_{\text{C=O}}$	$\nu_{\text{(C-O-C)furan}}$	$\nu_{\text{M-O}}$	$\nu_{\text{M-N}}$	$\nu_{\text{M-Cl}}$
HL	3364br	—	1,623 m	1,214 m	1,024 m	—	—	—
[CoL(H ₂ O)Cl].2H ₂ O	—	3318 br	1,601 m	1,202 m	1,008 m	376 m	355 w	262m
[NiL(H ₂ O)Cl].4H ₂ O	—	3320 br	1,600 m	1,200 m	1,009 s	380 s	348 w	274 w
[CuL(H ₂ O)Cl].3H ₂ O	—	3320 br	1,601 s	1,203 m	1,012 m	363 m	352 m	267 m
[ZnL(H ₂ O)Cl].5H ₂ O	—	3300 br	1,600 m	1,203 m	1,010 m	365 m	345 m	277 m

br = broad; m = medium; s = small; sh = sharp; w = weak.

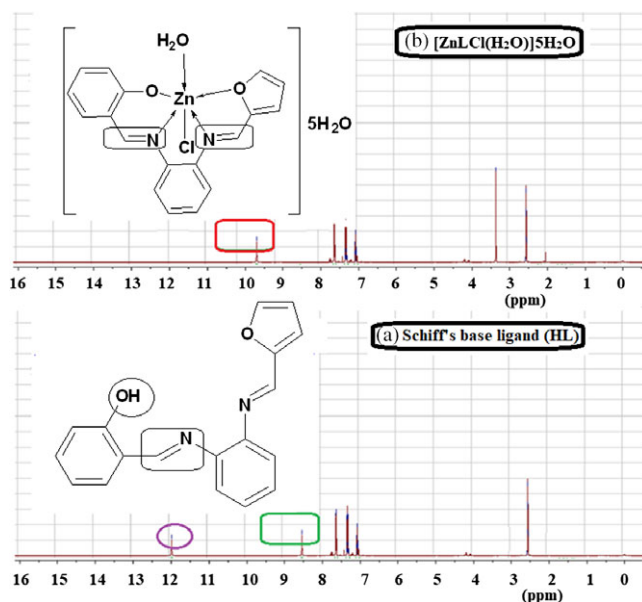


FIGURE 2 (a) ^1H NMR spectrum of furan-Schiff base HL ligand. (b) ^1H NMR spectrum of the $[\text{ZnL}(\text{H}_2\text{O})\text{Cl}]\cdot 5\text{H}_2\text{O}$ complex

3.1.3 | NMR spectra

The ^1H NMR data of the HL ligand (Figure 2a) shows that the tautomeric equilibrium favors the enol-imine in DMSO. The broad signal at $\delta = 11.93$ ppm is assigned to the proton of the hydroxyl group. This signal is due to the hydrogen-bonded phenolic proton, and the integration is generally less than 2.0 due to this intramolecular hydrogen bonding. The signal due to the azomethine ($\text{CH}=\text{N}$) proton of the characteristic azomethine group for azomethine Schiff base $-\text{N}=\text{C}(\text{H})-$ was observed at 8.57 ppm. In the region 6.88–7.37 ppm, the chemical shifts were assigned to the hydrogen of the aromatic ring. In the ^{13}C NMR spectrum of the HL ligand (Figure S2), azomethine carbon is at 160.12 ppm.

3.2 | UV spectrum

The UV spectra of the azomethine furan-Schiff base HL ligand in ethanol, dichloromethane, acetonitrile, and hexane show absorption bands at 224, 232, 257, and 262 nm, which are assigned to the $\pi \rightarrow \pi^*$ transitions of the enol-imine tautomer of the ligand. The observed small hypsochromic shift of the 332 nm band in more polar solvents is typical of the $n \rightarrow \pi^*$ transitions of the $\text{C}=\text{N}$ group. The maximum at 417 nm detected in EtOH solutions of the furan-Schiff base HL ligand is assigned to the $n \rightarrow \pi^*$ transitions in the dipolar zwitterionic or the keto-imine tautomeric structures.

3.3 | Mass spectrum

The electron impact (EI) mass spectrum (Figure S3) of the free azomethine furan-Schiff base HL ligand confirms the proposed formula by showing a peak at 280 u corresponding to the ligand moiety $[(\text{C}_{18}\text{H}_{14}\text{N}_2\text{O}_2)]$ atomic mass 290 u]. The series of peaks in this range, namely 52, 82, 118,

148, 152, 208, and 227 u, are attributable to different fragments of the furan-Schiff's base HL ligand. These data suggest the condensation of the keto ($-\text{C}=\text{O}$) group with the amino ($-\text{NH}_2$) group. The molecular ion peak of azomethine furan-Schiff base HL ligand (290 u) is in good agreement with the proposed molecular formula indicated from elemental analyses.

3.4 | Characterization of the furan-Schiff base metal complexes

On the basis of analytical data (Table 1), all the furan-Schiff base metal(II) complexes have the general composition $[\text{ML}(\text{H}_2\text{O})\text{Cl}]\cdot n\text{H}_2\text{O}$ $\{\text{L} = 2\text{-furan-2-ylmethyleneaminophenyliminomethyl-phenol}$ and for $\text{M} = \text{Co}(\text{II})$, $n = 2$; $\text{Ni}(\text{II})$, $n = 4$; $\text{Cu}(\text{II})$, $n = 3$; and $\text{Zn}(\text{II})$, $n = 5\}$. The obtained furan-Schiff base complexes are powders, which are stable in air and decompose above 300°C (Table 1). They are soluble in organic solvents such as acetone, chloroform, methanol, DMF, and DMSO but insoluble in most nonpolar solvents. The Λ_m (molar conductance) values of the soluble related furan-Schiff's base metal(II) complexes (**1–4**) in dimethylformamide (DMF) are in the range $6.54\text{--}9.12 \Omega^{-1} \text{cm}^2 \text{mol}^{-1}$, indicating their non-electrolyte nature.^[23]

3.5 | IR spectra

In the IR spectra of the furan-Schiff base HL ligand (Figure S1; Table 2), the absorption at 1623cm^{-1} is attributed to the presence of the azomethine group ($-\text{CH}=\text{N}$). The shifting of this band to lower frequencies (by 23cm^{-1}) in all the corresponding furan-Schiff base metal(II) complexes indicate the coordination of the azomethine nitrogen ($-\text{C}=\text{N}$) to the metal ion, which can be explained by the donation of electrons from the nitrogen to the empty d orbital of the metal ion. A broad band at 3364cm^{-1} is observed, which is due to the phenolic OH group, and disappears in the spectra of all furan-Schiff base metal(II) complexes, suggesting the deprotonation of the phenolic OH group by the metal ion. The band observed at 1214cm^{-1} is assigned to phenolic C–O stretching vibration, which gets shifted to lower frequencies in all the corresponding furan-Schiff base metal(II) complexes and is consistent with coordination via the protonated phenolic oxygen.^[24] Also, the specific band of the $\nu(\text{C}-\text{O}-\text{C})$ furan ring vibration at 1024cm^{-1} in the ligand shifts to $1,008\text{--}1,012 \text{cm}^{-1}$ in all furan-Schiff base metal(II) complexes.^[24] The bands observed in the ranges 380–363, 355–345, and 262–277 may be assigned to (M–O), (M–N), and (M–Cl), respectively.^[24]

3.5.1 | NMR spectral data

The ^1H NMR spectroscopic data of the furan-Schiff base HL ligand (Figure 2a) and its $[\text{ZnL}(\text{H}_2\text{O})\text{Cl}]\cdot 5\text{H}_2\text{O}$ complex (Figure 2b) were collected in $\text{DMSO-}d_6$. The broad signal at 11.93 ppm is due to the $-\text{OH}$ proton in the furan-Schiff's

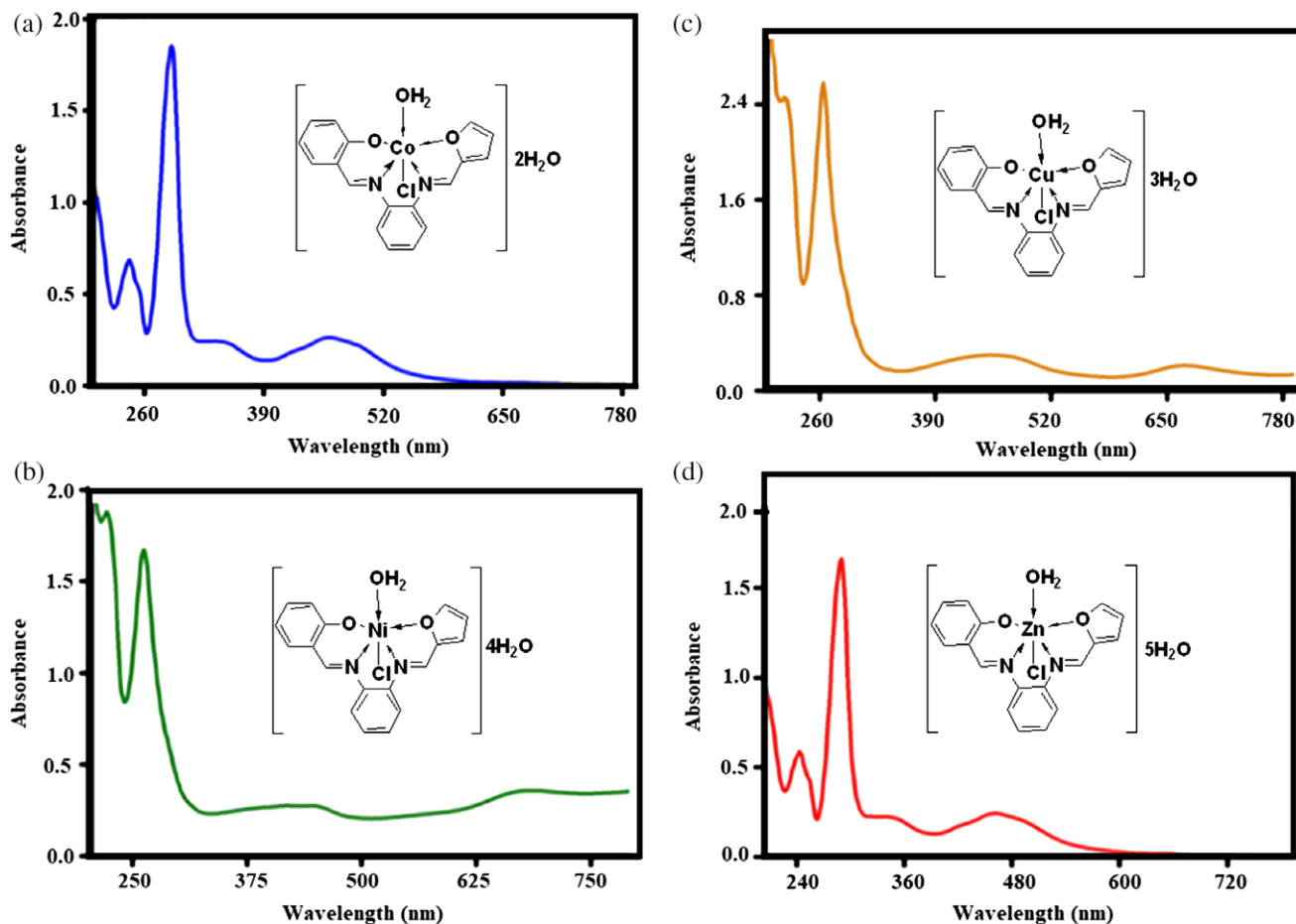


FIGURE 3 Electronic spectra of the (a) $[\text{CoL}(\text{H}_2\text{O})\text{Cl}]\cdot 2\text{H}_2\text{O}$ complex, (b) $[\text{NiL}(\text{H}_2\text{O})\text{Cl}]\cdot 4\text{H}_2\text{O}$ complex, (c) $[\text{CuL}(\text{H}_2\text{O})]\cdot 3\text{H}_2\text{O}$ complex, and (d) $[\text{ZnL}(\text{H}_2\text{O})]\cdot 5\text{H}_2\text{O}$ complex

base HL ligand, and the disappearance of the signal due to the $-\text{OH}$ proton in the spectrum of the $[\text{ZnL}(\text{H}_2\text{O})]\cdot 5\text{H}_2\text{O}$ complex supported the protonation of the thiol group. The signal of the azomethine proton is shifted to high field in the spectrum of the $[\text{ZnL}(\text{H}_2\text{O})\text{Cl}]\cdot 5\text{H}_2\text{O}$ complex. It appears at 9.88 ppm as compared to 8.57 ppm in the furan-Schiff base HL ligand. This indicates complexation to the zinc atom through the azomethine nitrogen atom. The ^1H NMR spectrum of the furan-Schiff base HL ligand shows a multiplet at 7.24–7.73 ppm due to aromatic protons. The signal observed at 3.13 ppm with an

integration corresponding to 12 protons in the case of $[\text{ZnL}(\text{H}_2\text{O})\text{Cl}]\cdot 5\text{H}_2\text{O}$ complex was assigned one coordinate and five hydrate and one coordinate water molecules. The ^1H NMR spectra of the furan-Schiff base HL ligand and of the $[\text{ZnL}(\text{H}_2\text{O})\text{Cl}]\cdot 5\text{H}_2\text{O}$ complex are given in Figure 2a and b.

In the ^{13}C NMR of the furan-Schiff base HL ligand (Figure S2), the $(-\text{C}=\text{N}-)$ azomethine carbon showed a signal at 160.12 ppm,^[25] the $(-\text{C}-\text{O}-)$ phenolic group carbon at 163.27 ppm,^[26] and the $(\text{C}-\text{O})$ furan ring at 170.12.^[27] The signals due to $(-\text{C}=\text{N}-)$ azomethine, $(-\text{C}-\text{O}-)$ phenolic, and

TABLE 3 Molar conductance, magnetic moment, and electronic spectral data of the complexes

Complex	Geometry	μ_{eff} (BM)	Band assignments	λ_{max} (cm^{-1})
$[\text{CoL}(\text{H}_2\text{O})\text{Cl}]\cdot 2\text{H}_2\text{O}$	Octahedral	3.98	$^4\text{T}_1 \rightarrow ^4\text{T}_2(\text{F}) (\nu_1)$ $^4\text{T}_1 \rightarrow ^4\text{A}_2(\text{F}) (\nu_2)$ $^4\text{T}_1 \rightarrow ^4\text{T}_1(\text{P}) (\nu_1)$	10,696 15,191 25,067
$[\text{NiL}(\text{H}_2\text{O})\text{Cl}]\cdot 4\text{H}_2\text{O}$	Tetrahedral	2.92	$^3\text{A}_2(\text{F}) \rightarrow ^3\text{T}_2(\text{F}) (\nu_2)$ $^3\text{A}_2(\text{F}) \rightarrow ^3\text{T}_1(\text{F}) (\nu_3)$ $^3\text{A}_2(\text{F}) \rightarrow ^3\text{T}_1(\text{P}) (\nu_3)$	11,357 15,803 21,489
$[\text{CuL}(\text{H}_2\text{O})\text{Cl}]\cdot 3\text{H}_2\text{O}$	Octahedral	2.06	$^2\text{B}_{1g} \rightarrow ^2\text{A}_{1g}(\text{dx}^2 - \text{y}^2 \rightarrow \text{dz}^2) (\nu_1)$ $^2\text{B}_{1g} \rightarrow ^2\text{A}_{2g}(\text{dx}^2 - \text{y}^2 \rightarrow \text{dz}^2) (\nu_2)$	18,534 30,373
$[\text{ZnL}(\text{H}_2\text{O})\text{Cl}]\cdot 5\text{H}_2\text{O}$	Octahedral	Diamagnetic	LMCT(M \leftarrow N)	25,674

TABLE 4 Ligand field parameters of the complexes

Complex	Dq (cm^{-1})	B (cm^{-1})	β	LFSE (kJ mol^{-1})	F_2	F_4	C	ν_2/ν_1
$[\text{Co}(\text{L})(\text{H}_2\text{O})\text{Cl}]\cdot 2\text{H}_2\text{O}$	1168	808	0.73	100.47	—	—	—	1.42
$[\text{Ni}(\text{L})(\text{H}_2\text{O})\text{Cl}]\cdot 4\text{H}_2\text{O}$	792	—	0.95	114.23	—	—	—	1.39
$[\text{Cu}(\text{L})(\text{H}_2\text{O})\text{Cl}]\cdot 3\text{H}_2\text{O}$	—	—	—	—	—	—	—	2.00

(C–O) furan carbons were slightly shifted downfield in comparison to the corresponding signals of these groups in the ligand, thereby confirming the complexation with the zinc metal ion. It was observed that DMSO did not have any coordinating effect on the spectrum of the $[\text{ZnL}(\text{H}_2\text{O})\text{Cl}]\cdot 5\text{H}_2\text{O}$ complex (Figure S2). The ^1H and ^{13}C NMR spectra of the furan-Schiff base HL ligand and $[\text{Zn}(\text{L})(\text{H}_2\text{O})]\cdot 5\text{H}_2\text{O}$ mononuclear complex are given in Figures 3 and S2.

3.5.2 | Mass spectra

The mass spectra of the furan-Schiff base metal(II) complexes (Figure S3) and the molecular ion peaks at 437, 473, 460, and 498 for corresponding furan-Schiff base metal(II) complexes were used to confirm the proposed formula (437, 473, 460, and 498u for Co(II), Ni(II), Cu(II), and Zn(II) complexes, respectively). The multippeak pattern of the mass spectrum gives an impression of the successive degradation of the target compound, with the series of peaks corresponding to the various fragments. Their intensity gives an idea of the stability of the fragments. The last four fragments in all the complexes appear at positions (m/z value) 158 (100%), 144 (<100%), 120 (<100%), and 144 (<100%). These values correspond to

the $[\text{C}_5\text{H}_9\text{NOCu}]^+$, $[\text{C}_5\text{H}_{10}\text{ONi}]^+$, $[\text{C}_3\text{H}_5\text{OCu}]^+$, and $[\text{C}_3\text{H}_{11}\text{O}_2\text{Zn}]^+$ fragments, respectively.

3.5.3 | Electronic, ligand field parameters, and magnetic susceptibility measurements

The electronic spectrum of the Co(II) complex (Figure 3a; Table 3) shows three bands at 10,696, 15,191, and 25,067 cm^{-1} . These bands may be assigned to following transitions: $^4\text{T}_{1g} \rightarrow ^4\text{T}_{2g}$ (F) (ν_1), $^4\text{T}_{1g} \rightarrow ^4\text{A}_{2g}$ (F) (ν_2), and $^4\text{T}_{1g} \rightarrow ^4\text{T}_{1g}$ (P) (ν_3), respectively. The positions of the bands suggest octahedral geometry of the Co(II) complex.^[28] The Co(II) complex shows a magnetic moment of 3.98 BM, corresponding to the three unpaired electrons. The ligand field parameters were calculated for the cobalt(II) complex. The value of Dq was calculated from Orgel energy level diagrams using the ν_3/ν_1 ratio.^[29] The value for B (free ion) is 1,126 cm^{-1} . The value of β indicates that the covalent character of metal ligand σ -bond is low (Table 4).

The electronic spectrum of the Ni(II) complex (Figure 3b; Table 3) displays bands at 11,357, 15,803, and 21,489 cm^{-1} , and may be assigned to the $^3\text{A}_{2g}(\text{F}) \rightarrow ^3\text{T}_{2g}$ (F) (ν_1), $^3\text{A}_{2g}(\text{F}) \rightarrow ^3\text{T}_{1g}(\text{F})$ (ν_2), and $^3\text{A}_{2g}(\text{F}) \rightarrow ^3\text{T}_{1g}$ (P) (ν_3) transitions, respectively. It suggests the octahedral geometry of the Ni(II) complex.^[29] The nickel(II) complex shows a magnetic moment 2.92 BM, corresponding to two unpaired electrons.^[30]

Electronic spectrum of the copper(II) complex (Figure 3c; Table 3) displays bands at 14,992, 18,534 and 30,373 cm^{-1} . The first two bands may be assigned to the transitions $^2\text{B}_{1g} \rightarrow ^2\text{A}_{1g}$ ($dx^2 - y^2 \rightarrow dz^2$) (ν_1) and $^2\text{B}_{1g} \rightarrow ^2\text{B}_{2g}$ ($dx^2 - y^2 \rightarrow dzy$) (ν_2), respectively, and third band may be due to charge transfer. The observed magnetic moment of the Cu(II) complex is 1.96 BM, which confirms the octahedral structure of this complex.^[30]

The Zn(II) complex (Figure 3d; Table 3) is diamagnetic as expected, and its geometry is most probably octahedral similar to the Cu(II), Co(II), and Ni(II) complexes of the HL ligand.

3.5.4 | EPR spectrum of $[\text{CuL}(\text{H}_2\text{O})\text{Cl}]\cdot 3\text{H}_2\text{O}$ complex

The solid-state ESR spectrum of the $[\text{CuL}(\text{H}_2\text{O})\text{Cl}]\cdot 3\text{H}_2\text{O}$ complex (Figure 4a, Table 5) was recorded at room temperature. The shape of the spectrum is consistent with the

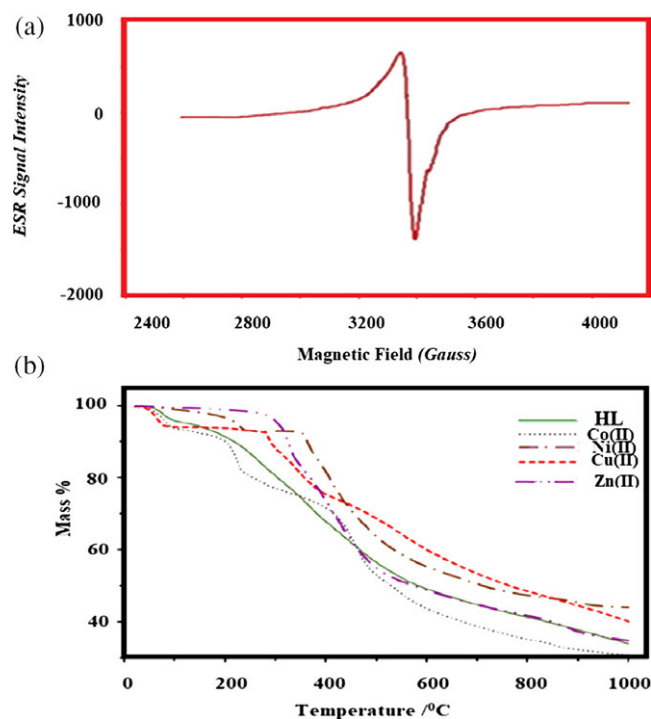


FIGURE 4 (a) EPR spectrum of the $[\text{CuL}(\text{OH}_2)]\cdot 3\text{H}_2\text{O}$ complex. (b) TGA spectra of the furan-Schiff's base ligand (HL) and its metal complexes (1–4)

TABLE 5 EPR bonding parameters of Cu(II) complex at room temperature

Complex	α^2	β^2	γ^2	G	K_{\parallel}	K_{\perp}
$[\text{CuL}(\text{H}_2\text{O})\text{Cl}]\cdot 3\text{H}_2\text{O}$	0.7235	0.7365	0.6287	4.63	0.7369	0.2348

TABLE 6 Crystallographic data for the Schiff base complexes [CoLCl(H₂O)].2H₂O, [NiLCl(H₂O)].4H₂O, [CuLCl(H₂O)].3H₂O, and [ZnLCl(H₂O)].5H₂O

Data	[CoLCl(H ₂ O)].2H ₂ O	[NiLCl(H ₂ O)].4H ₂ O	[CuLCl(H ₂ O)].3H ₂ O	[ZnLCl(H ₂ O)].5H ₂ O
Empirical formula	C ₁₈ H ₁₉ ClN ₂ O ₃ Co	C ₁₈ H ₂₄ ClN ₂ O ₇ Ni	C ₁₈ H ₂₁ ClN ₂ O ₆ Cu	C ₁₈ H ₂₅ ClN ₂ O ₈ Zn
Formula weight (g/mol)	437.7	473.5	460.4	498.2
Wavelength (Å)	0.71073	0.71073	1.54056	1.54056
Crystal system	Triclinic	Monoclinic	Orthorhombic	Triclinic
Space group	P $\bar{1}$	P2(1)/c	Pbca	P $\bar{1}$
a (Å)	5.6934(3)	9.2066(7)	12.287 (5)	7.9981(5)
b (Å)	9.3416(5)	19.1090(13)	11.884 (5)	12.6314(8)
c (Å)	12.6415(7)	18.589(2)	37.152 (5)	19.4346(10)
α (°)	116.513(6)	90	90	91.140(4)
β (°)	92.160(5)	100.46(3)	90	96.019(4)
γ (°)	102.669(5)	90	90	113.464(5)
Volume (Å ³)	3,266.2(4)	3,266.2(4)	5,425	856.46
(Calc.) density (g/cm ⁻³)	1.557	1.557	1.543	1.701
2 θ range	1.71–28.27	1.71–28.27	10.25–67.27	12.56–68.00
Limiting indices	–16 $\leq h \leq$ 6 –15 $\leq k \leq$ 5 –15 $\leq l \leq$ 5	–6 $\leq h \leq$ 7 –34 $\leq k \leq$ 34 –12 $\leq l \leq$ 9	0 $\leq h \leq$ 15 0 $\leq k \leq$ 15 0 $\leq l \leq$ 47	–10 $\leq h \leq$ 10 –12 $\leq k \leq$ 12 –25 $\leq l \leq$ 25
Z	2	4	8	2
Number of reflections	14,623	14,354	14,258	13,567
Number of independent reflections/parameters	164/2814	323/2537	332/2756	342/2428
R _{int}	0.0266	0.0224	0.078	1.004
Goodness-of-fit S	0.893	1.007	0.985	0.858
R (all data)/R[F _o ² > 4 σ (F _o ²)]	0.0341/0.0222	0.0362/0.0213	0.0290/0.0219	0.0479/0.0238
wR ₂ (all data)	0.048	0.039	0.0322	0.0723
Temperature (K)	298	298	298	298

octahedral environment around Cu(II) ion, and the higher *g*-value of the investigated [CuL(H₂O)Cl].3H₂O complex, when compared to that of a free electron (*g* = 2.24), reveals an appreciable covalency of the metal ligand bonding with

*d*_{x₂-y₂} as the ground-state characteristic of octahedral stereochemistry.^[31] Also, the *g*_{||}/*A*_{||} value of 143 for the [CuL(H₂O)Cl].3H₂O complex lies just within the range expected for the octahedral complex.^[31] The decrease of the *g*-value

TABLE 7 Thermal analyses data for furan-Schiff's base ligand (HL) and the corresponding metal complexes (1–4)

Compound	Temp. range (°C)	Calc. mass loss (found) %	Assignment
HL	50–125	32.41 (32.38)	Loss of phenol
	125–205	23.45 (23.42)	Loss of furan
	205–395	37.23 (37.21)	Loss of C ₅ H ₄ N ₂ O
	395–999	12.40 (12.37)	Loss of carbon atoms
[Co(L)(H ₂ O)Cl].2H ₂ O	100–190	16.33 (15.31)	Loss of 2H ₂ O (hydrated) + 1/2Cl ₂
	190–330	4.11 (4.08)	Loss of H ₂ O (coordinated)
	330–898	57.69 (57.94)	Loss of C ₁₈ H ₁₃ N ₂ O
	>900	17.11 (17.09)	CoO
[Ni(L)(H ₂ O)Cl].4H ₂ O	100–188	22.70 (22.68)	Loss of 4H ₂ O (hydrated) + 1/2Cl ₂
	170–340	3.80 (3.78)	Loss of H ₂ O (coordinated)
	340–899	57.72 (57.69)	Loss of C ₁₈ H ₁₃ N ₂ O
	>900	15.77 (15.75)	NiO
[Cu(L)(H ₂ O)Cl].3H ₂ O	100–189	19.43 (19.41)	Loss of 3H ₂ O (hydrated) + 1/2Cl ₂
	160–360	3.91 (3.87)	Loss of H ₂ O (coordinated)
	360–897	59.36 (59.32)	Loss of C ₁₈ H ₁₃ N ₂ O
	>900	17.26 (17.23)	CuO
[Zn(L)(H ₂ O)Cl].5H ₂ O	100–190	25.19 (25.16)	Loss of 5H ₂ O (hydrated) + 1/2Cl ₂
	160–340	3.61 (3.57)	Loss of H ₂ O (coordinated)
	340–898	54.85 (54.82)	C ₁₈ H ₁₃ N ₂ O
	>900	16.33 (16.30)	ZnO

TABLE 8 Kinetic parameters of the furan-Schiff's base ligand (HL) and their corresponding metal(II) complexes

Compound	Decomposition temperature (°C)	Method	Parameters					Correlation coefficient
			E_a (kJ/mol ⁻¹)	A (s ⁻¹)	ΔS^\ddagger (J mol ⁻¹ K ⁻¹)	ΔH^\ddagger (kJ/mol)	ΔG^\ddagger (kJ/mol)	
.HL	122–447	CR	28.4	5.2	–247	24.2	164	0.9977
		HM	38.1	6.5	–235	33.3	169	0.9972
		PN	28.6	5.8	–241	31.8	165	0.9974
[Co(L)(H ₂ O)Cl].2H ₂ O	142–372	CR	38.9	162	–203	54.2	162	0.9924
		HM	42.3	163	–207	55.6	165	0.9928
		PN	41.7	162	–205	56	163	0.9929
[Ni(L)(H ₂ O)Cl].4H ₂ O	175–315	CR	62.9	172	–223	63.2	158	0.9897
		HM	63.2	173	–222	64.8	155	0.9895
		PN	62.7	174	–224	63.8	157	0.9898
[Cu(L)(H ₂ O)Cl].3H ₂ O	193–347	CR	68.8	180	–238	54.2	167	0.9896
		HM	68.3	182	–236	64.8	166	0.9899
		PN	69.1	179	–237	65.2	164	0.9897
[Zn(L)(H ₂ O)Cl].5H ₂ O	187–374	CR	66.6	169	–242	64.7	159	0.9887
		HM	67.2	170	–244	55.8	158	0.9888
		PN	66.8	171	–243	56.3	157	0.9885

CR = Coats–Redfern; HM = Horowitz–Metzger; PN = Piloyan–Novikova.

by 9 compared to that of the free-electron value (2.07) is an approximate measure of the ligand field strength; the stronger the furan-Schiff's base ligand field, the smaller the decrease in the g -value, and vice versa.

3.5.5 | Powder XRD

Single crystals of the corresponding furan-Schiff's base metal complexes could not be obtained. The cell parameters (Figure S4; Table 6) were determined using X-ray powder

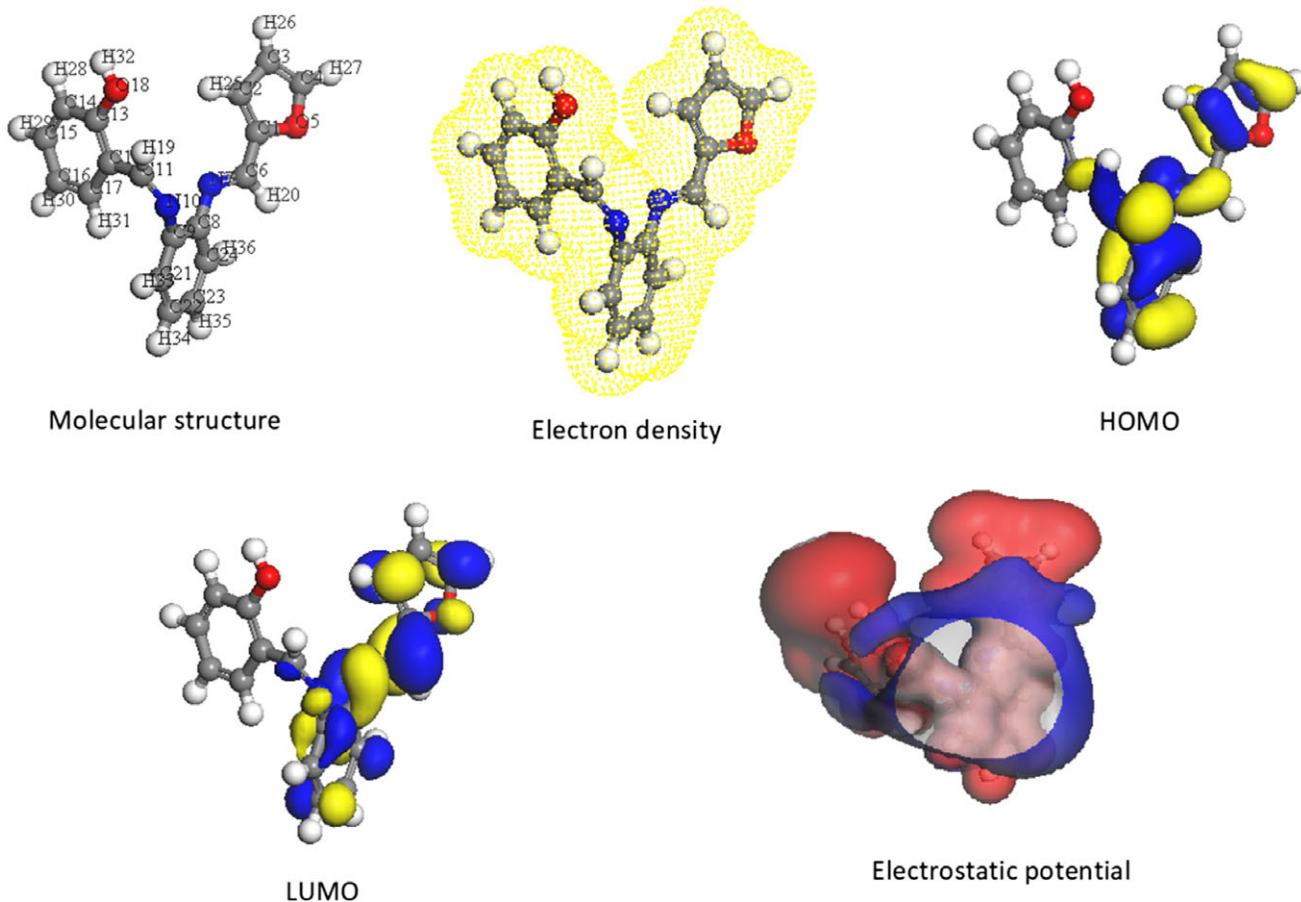


FIGURE 5 Molecular structure, electron density, HOMO, LUMO, and electrostatic potential of the ligand HL

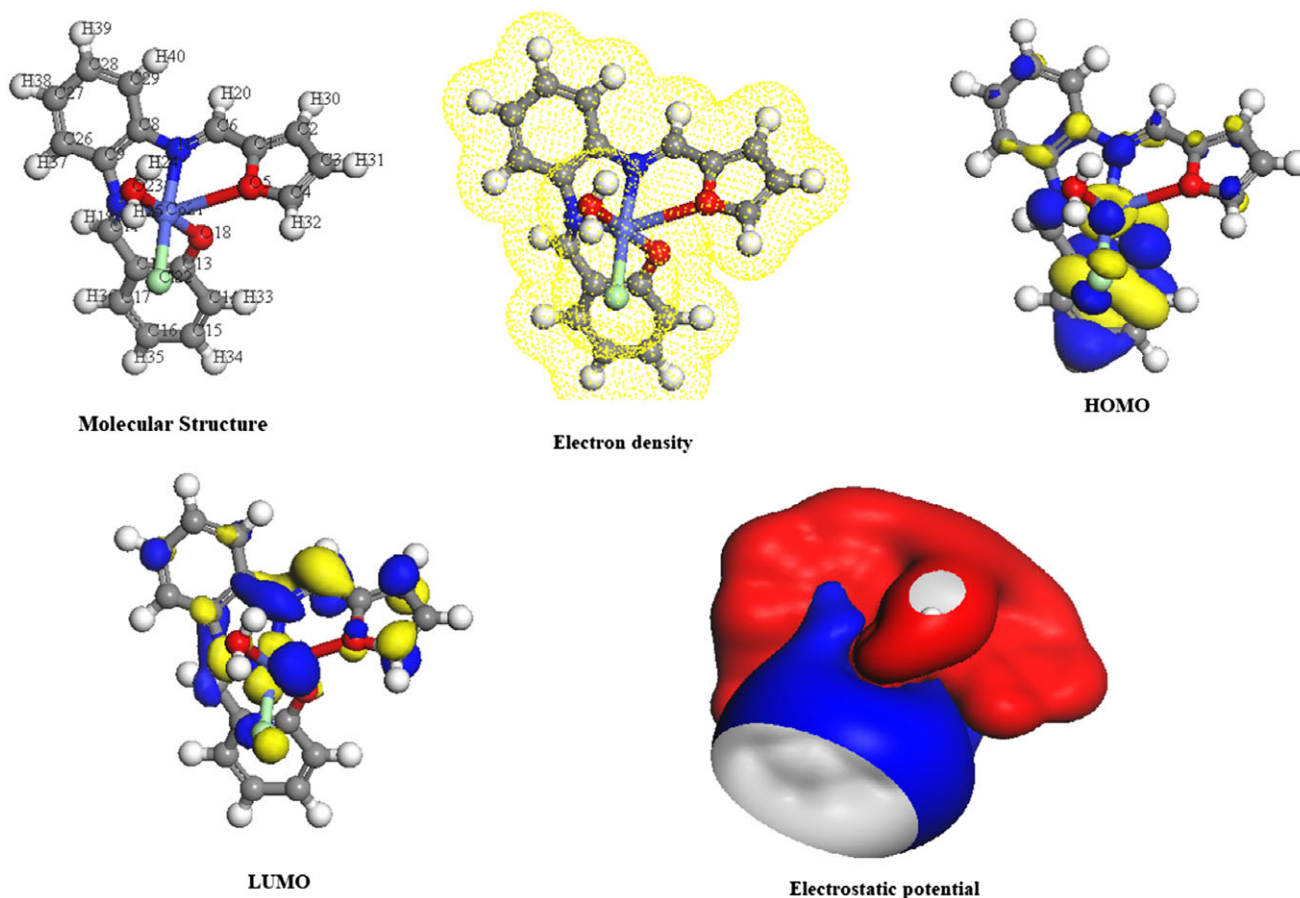


FIGURE 6 Molecular structure, electron density, HOMO, LUMO, and electrostatic potential of the $\text{Co}^{\text{II}}\text{-L}$ complex

diffraction data. The indexing was carried out using the (CCP4, UK) CRYSFIRE program^[32] for the $[\text{CoL}(\text{H}_2\text{O})\text{Cl}]\cdot 2\text{H}_2\text{O}$, $[\text{NiL}(\text{H}_2\text{O})\text{Cl}]\cdot 4\text{H}_2\text{O}$, $[\text{CuL}(\text{H}_2\text{O})\text{Cl}]\cdot 3\text{H}_2\text{O}$, and $[\text{ZnL}(\text{H}_2\text{O})\text{Cl}]\cdot 5\text{H}_2\text{O}$ complexes, giving triclinic, monoclinic, orthorhombic, and orthorhombic crystal systems, respectively.

3.5.6 | Thermal analysis

The thermal properties of the furan-Schiff's base ligand (HL) and the corresponding metal(II) complexes (**1–4**) were characterized on the basis of thermogravimetric analysis (TGA) results. The TGA curves are given in Figure 4b, and the data are listed in Table 7. The weight losses for each compound were calculated within the corresponding temperature ranges.

The furan-Schiff base ligand (HL) shows four decomposition steps. The first stage occurs in the temperature range 50–125 °C and is attributed to the loss of the phenol moiety (found 32.38% and calc. 32.41%). The second stage in the temperature range 125–205 °C corresponds to the loss of furan (found 23.42%, calc. 23.45%). The third stage in the temperature range 205–395 °C corresponds to the loss of a part of the ligand ($\text{C}_5\text{H}_4\text{N}_2\text{O}$) (found 37.21%, calc. 37.23%). The fourth stage occurs in the temperature range 395–999 °C, corresponding to the loss of carbon atoms (found 22.1%, calc. 22.00%).

The $\text{Co}(\text{II})$, $\text{Ni}(\text{II})$, $\text{Cu}(\text{II})$, and $\text{Zn}(\text{II})$ complexes showed TG curves in the temperature range ~100–190 °C corresponding to the loss of two, four, three, and five hydrated water molecules + 1/2 Cl_2 molecule. The second stage is related to the loss of one molecule of the coordinated water for the metal(II) complexes ($\text{Co}(\text{II})$, $\text{Ni}(\text{II})$, $\text{Cu}(\text{II})$, and $\text{Zn}(\text{II})$). The third stage is related to the loss of the part of furan-Schiff base ligand (HL). The final weight losses are due to the decomposition of the rest of the ligand and metal(II) oxide residue.

3.5.7 | Kinetic studies

The thermodynamic activation parameters (Table 8) of decomposition processes of the furan-Schiff base metal(II) complexes, namely the activation energy (E^*), entropy (ΔS^*), and Gibbs free energy change of the decomposition (ΔG^*), were evaluated graphically by employing three methods, that is, those of Coats–Redfern^[33] (CR), the Horowitz–Metzger^[34] (HM), and the Piloyan–Novikova^[35] (PN). From the results obtained, the following remarks can be made:

1. The energy of activation (E) increases on going from one decomposition stage to another for a given complex, indicating that the rate of decomposition decreases in the same order. Generally, stepwise stability constants

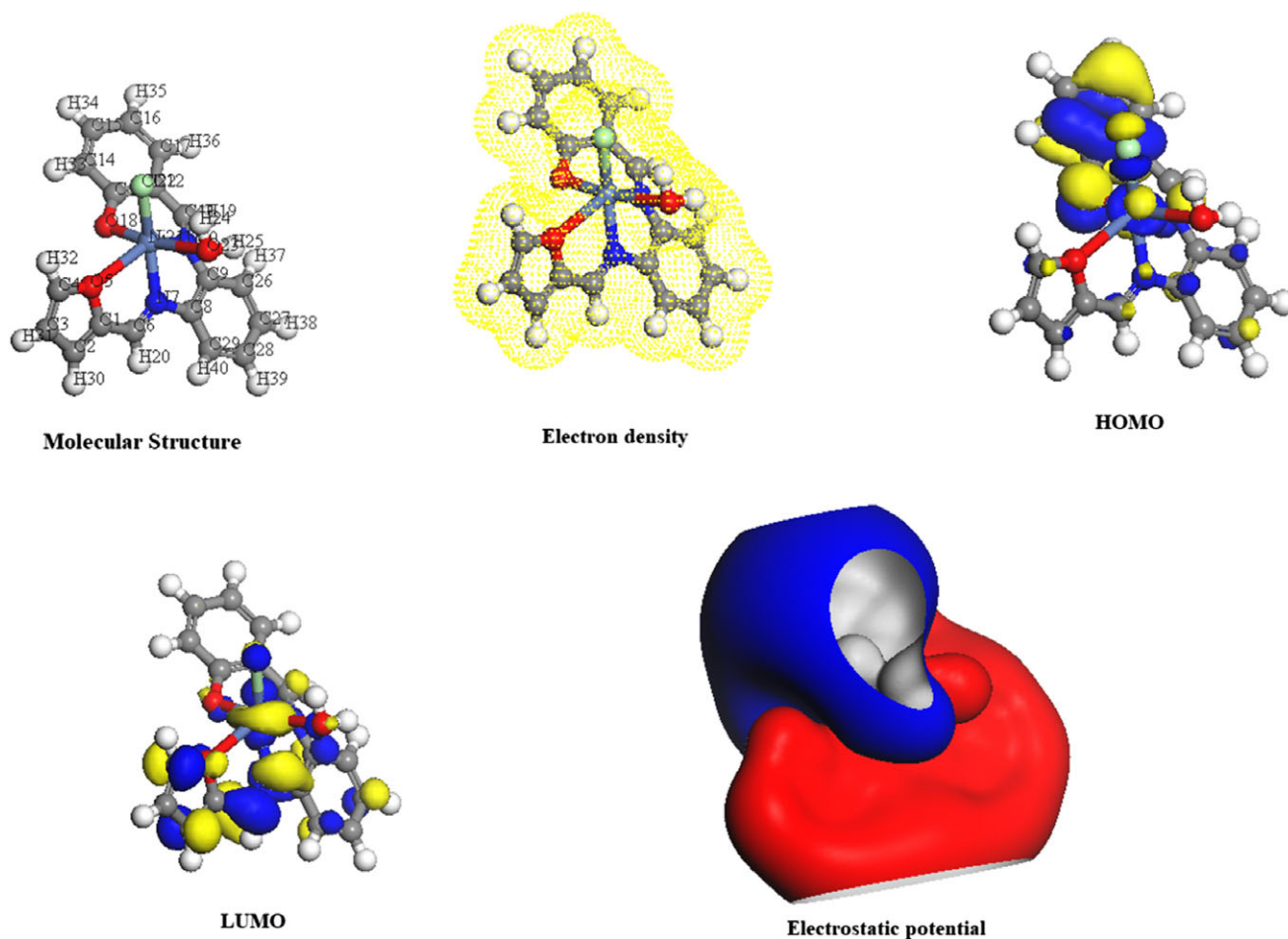


FIGURE 7 Molecular structure, electron density, HOMO, LUMO and electrostatic potential of the Ni^{II}-L complex

decrease with the increase in the number of ligands attached to a metal ion. Conversely, during the decomposition reaction, the rate of removal of the remaining ligands will be smaller after the expulsion of the furan-Schiff's base ligand (HL).^[36]

2. The ΔG values increase significantly for the subsequent decomposition stages because of the increase in the $T\Delta S$ values from one stage to another. This may be attributed to the structural rigidity of the remaining complex after the expulsion of more ligands, as compared with the precedent complex, which requires more energy, $T\Delta S$, for its rearrangement before undergoing any compositional change.^[36]
3. The negative ΔS values for the decomposition steps indicate that all the studied metal(II) complexes are more ordered in their activated states.^[37]
4. The positive ΔH values mean that the decomposition processes are endothermic.^[37]

3.5.8 | Molecular modeling

Molecular modeling gives a blueprint of the three-dimensional arrangement of atoms of any compound. The

theoretical physical parameters such as bond length, bond angles, highest occupied molecular orbital (HOMO), and lowest unoccupied molecular orbital (LUMO) were recorded using the Accelrys Material Studio.^[38]

If any deviations in the bond distance, bond angle, or torsion angle, are evidenced, specific electronic interactions can be detected, confirming the earlier spectral evidences.^[39] Thus, the physical dimension of the molecules helps to demonstrate the changes occurring during their topological assemblies.

The deprotonated furan-Schiff base ligand (HL) (Figure 1) is coordinated as a tetradentate ligand via the carbonyl oxygen, the two azomethine nitrogen atoms, and the oxygen of the furan ring. The coordination number of 6 is completed by one chlorine with one water molecule of the metal ions (Co^{II}, Ni^{II}, Cu^{II}, and Zn^{II}).

The molecular structures, along with atom numbering, electron density, HOMO, LUMO, and electrostatic potential of the furan-Schiff's base ligand (HL), are depicted in Figure 5, whereas the same parameters are represented for the metal complexes in Figures 5–9.

Comparisons between the bond lengths and bond angles of the ligand and those of the Co^{II}, Ni^{II}, Cu^{II}, and Zn^{II} complexes are listed in Tables S1 and S2, respectively. Various

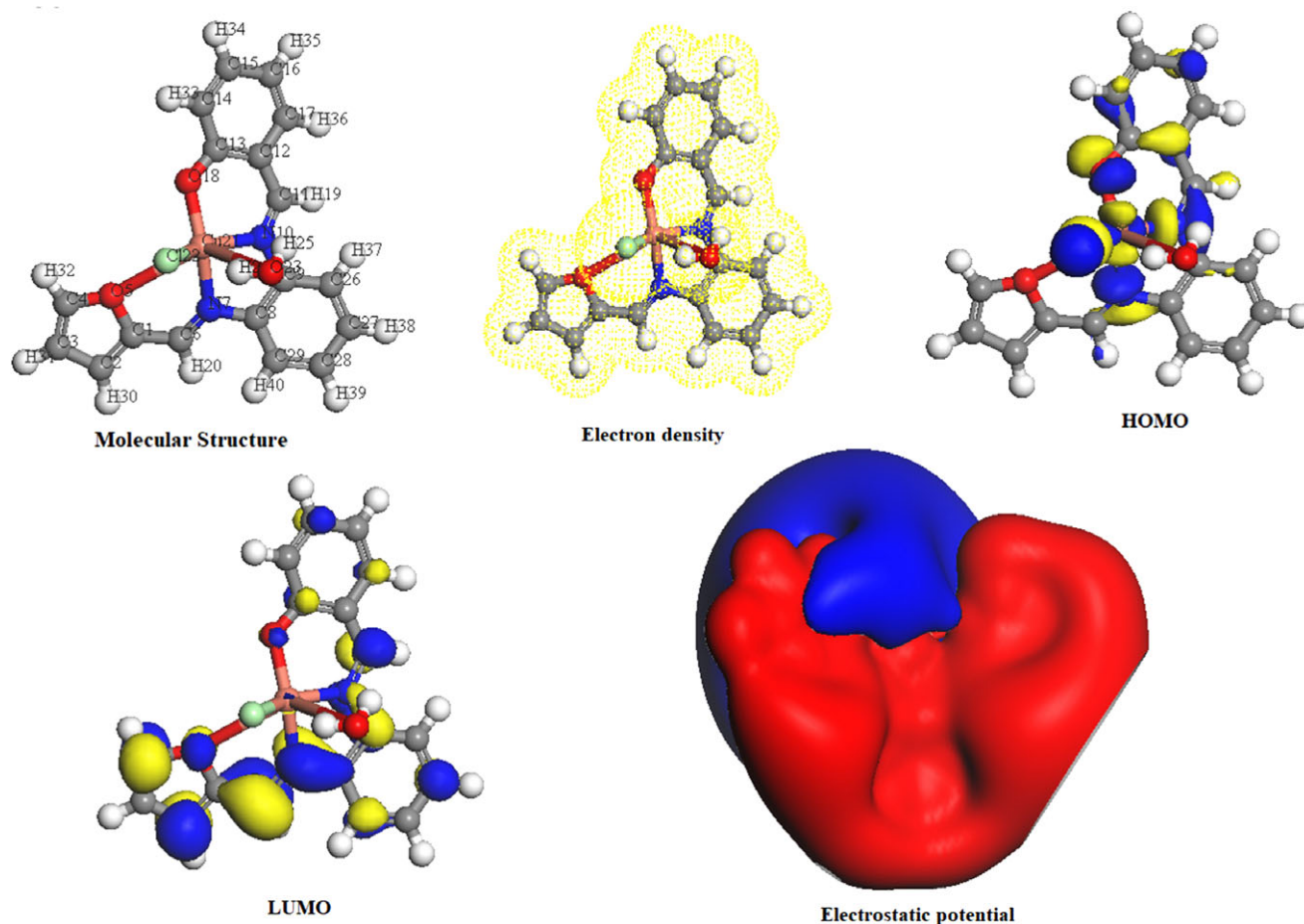


FIGURE 8 Molecular structure, electron density, HOMO, LUMO, and electrostatic potential of the $\text{Cu}^{\text{II}}\text{-L}$ complex

energetic data were calculated for the furan-Schiff's base ligand and its metal complexes and are shown in Tables S1 and S2. According to these data, many conclusions can be drawn:

- The actual bond angles and bond lengths are close to the optimal values, and thus the proposed structures of the compounds are acceptable.
- The bond lengths C(6)–N(7), C(9)–N(10), and N(10)–C(11) of the furan-Schiff base ligand were enlarged in the complexes as a result of the participation in coordination upon forming M–N(7) and M–N(10) bonds, whereas C(1)–O(5), C(4)–O(5), and C(13)–O(18) were mostly shortened but in some complexes enlarged upon coordination.
- The bond length O(18)–H(30) with the value 0.975 Å disappears upon coordination, as the ligand acts as a mono-negative tetradentate by losing this proton. Also, the value of the bond angle C(13)–O(18)–H(32), which is 108.184°, ensures the sp^3 hybridization of the oxygen atom which is an optimal assumption.
- This ligand's bond angles C(1)–O(5)–C(4), C(6)–N(7)–C(8), C(9)–N(10)–C(11), C(12)–C(13)–O(18), and C(14)–C(13)–O(18) are reduced or increased upon complexation.^[40]
- New bond angles were formed between the ligand and metal ions such as O(5)–M(21)–N(7), N(7)–M(21)–N(10), and N(10)–M(21)–O(18) with different values, ranging from 64.489° to 136.574°.^[41]
- The electrostatic potential is the energy of interaction of a point positive charge with the nuclei and electrons of a molecule, and its value depends on the location of the point positive charge (Table 9). Therefore, it is important to depict the structure of the electrostatic potential of the ligand and complexes.
- The complexes show octahedral geometry according to the values of the bond angles formed by the metal ion and the coordinated groups.
- The higher HOMO energy lies around the phenyl group, while the lower LUMO energy exists around the furan ring.
- A lower HOMO energy shows that the molecule's donating electron ability is weak. On the contrary, a higher HOMO energy implies that the molecule is a good electron donor. LUMO energy presents the ability of a molecule to receive an electron.^[42]

3.6 | Biological activity studies

3.6.1 | Antitumor activity

The HL ligand and its isolated metal(II) complexes were tested for antitumor activity against the colon carcinoma cell

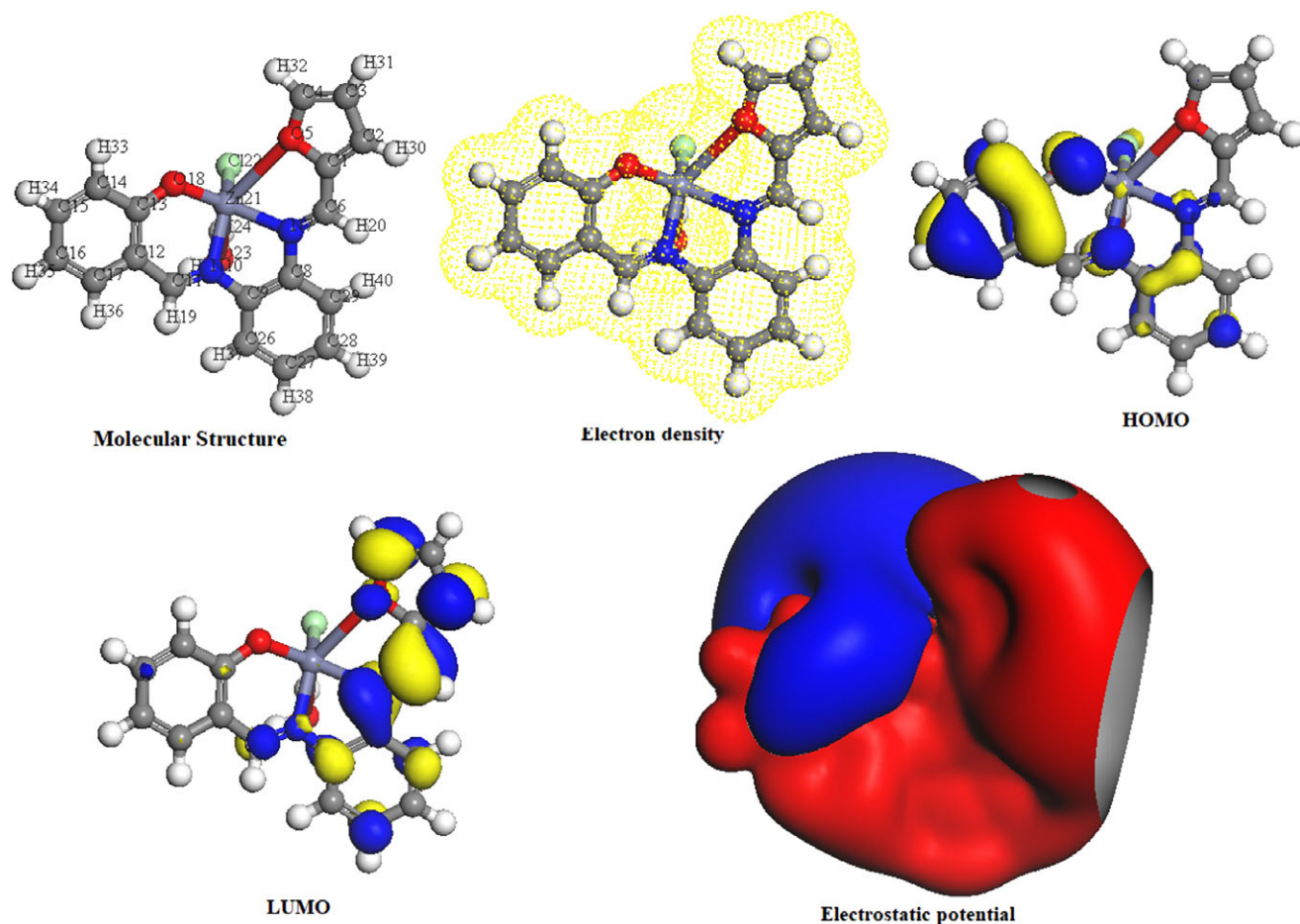


FIGURE 9 Molecular structure, electron density, HOMO, LUMO, and electrostatic potential of the Zn^{II} -L complex

TABLE 9 Some energetic data containing total energy, binding energy, dipole moment, HOMO, LUMO, ΔE_{Gap} , and electrostatic potential

Compd	Total energy (kcal/mol)	Binding energy (kcal/mol)	Dipole moment (D)	HOMO (eV)	LUMO (eV)	ΔE_{Gap}	Electrostatic potential (kcal/mol)
Ligand	-5.99×10^5	-4285.551	6.1027	-4.863	-2.454	2.411	-1160.707
Co^{II} -L	1.040×10^6	-4659.968	9.3964	-4.978	-3.398	1.58	-3539.32
Ni^{II} -L	-1.057×10^6	-4651.276	10.9206	-4.931	-3.413	1.518	-3319.623
Cu^{II} -L	-1.075×10^6	-4585.814	12.6023	-4.700	-3.322	1.378	-1001.360
Zn^{II} -L	-1.095×10^6	-4561.082	11.1595	-5.206	-3.326	1.88	-1731.549

TABLE 10 Cytotoxicity for the HL ligand and its isolated metal(II) complexes against human colorectal cancer cells (HCT-116)

Compd.	Cell viability % at different concentrations (μg)								IC_{50} ($\mu g/mL$) ^a
	0.0	1.56	3.125	6.25	12.50	25.00	50.00	100.0	
HL ligand	100.00	100	98.64	87.27	77.25	68.23	46.86	34.28	42.86
$Co(II)$	100.00	100	97.58	86.38	75.89	62.34	42.28	32.47	41.12
$Ni(II)$	100.00	100	96.26	82.16	70.12	56.56	35.69	21.88	28.22
$Cu(II)$	100.00	97.56	88.78	72.43	56.65	52.73	32.46	21.42	19.37
$Zn(II)$	100.00	94.98	84.53	85.86	72.45	59.41	39.87	26.74	17.61

^a IC_{50} is concentration that can reduce the growth of cancer cells by 50%.

(HCT-116) and the mouse myelogenous leukemia carcinoma (M-NFS-60) at various concentrations (100, 50, 25, 12.5, 6.25, 3.125, and 1.56 $\mu g/mL$). The anticancer efficiency of all the tested compounds is shown in Tables 10 and 11, whereas Figures S5 and S6 show the effect of different concentrations of all compounds under study on (HCT-116) and

(M-NFS-60), respectively. Additionally, the IC_{50} values derived from experimental data are summarized in Tables 10 and 11 and represented graphically in Figures S7 and S8. All the metal complexes were found to be cytotoxic against (HCT-116) and (M-NFS-60) and produced 50% cell death in the concentration range 17.51–42.86 $\mu g/mL$. Among the

TABLE 11 Cytotoxicity for the HL ligand and its isolated metal(II) complexes against leukemia cells (M-NFS-60)

Compd.	Cell viability % at different concentrations (μg)								IC_{50} ($\mu\text{g}/\text{mL}$) ^a
	0.0	1.56	3.125	6.25	12.50	25.00	50.00	100.0	
HL ligand	100	98.82	98.43	87.14	77.18	68.12	46.71	34.17	42.68
Co(II)	100	100	97.24	86.23	75.68	62.23	42.18	32.36	41.03
Ni(II)	100	98.92	96.14	82.02	70.02	56.46	35.57	21.72	28.15
Cu(II)	100	84.26	88.57	72.33	56.46	52.43	32.37	21.34	19.23
Zn(II)	100	97.58	84.42	85.74	72.32	59.34	39.63	26.62	17.53

^a IC_{50} is concentration that can reduce the growth of cancer cells by 50%.

TABLE 12 Antimicrobial screening results of the HL ligand and its isolated metal(II) complexes

Microorganisms	HL ligand	Co(II) complex	Ni(II) complex	Cu(II) complex	Zn(II) complex	Std.
Fungi						Amphotericin B
<i>Aspergillus Fumigatus</i> (RCMB 02568)	NA	NA	17.8	22.8	20.8	25.8
<i>Syncephalastrum racemosum</i> (RCMB 05922)	NA	NA	NA	NA	NA	20.7
<i>Geotricum candidum</i> (RCMB 05097)	NA	NA	12.8	20.8	16.8	29.4
<i>Candida tropicalis</i> (RCMB 05168)	NA	NA	NA	NA	NA	23.6
Gram-positive bacteria						Ampicillin
<i>Streptococcus pneumonia</i> (RCMB 010010)	NA	NA	12.2	16.4	15.8	23.6
<i>Bacillus subtilis</i> (RCMB 010067)	NA	5.6	15.7	18.4	17.4	23.5
Gram-negative bacteria						Ciprofloxacin
<i>Salmonella typhi</i> (RCMB 010072)	NA	NA	NA	NA	NA	22.7
<i>Escherichia coli</i> (RCMB 010052)	NA	NA	13.4	21.2	15.3	25.3

Note: Test was done using the diffusion agar technique; NA: No activity.

TABLE 13 Inhibition efficiencies of the isolated metal(III) complexes on carbon steel corrosion in 0.5 M HCl at 25 °C obtained by weight loss method

Time	C_{inh} (1.0×10^{-3} M)	HCl	HL ligand	Co(II) complex	Ni(II) complex	Cu(II) complex	Zn(II) complex
2	Rate $\times 10^{-2}$	8.00	7.85	6.36	6.23	6.78	3.34
	%Inhibition	—	3.84	12.45	21.05	19.24	34.21
4	Rate $\times 10^{-2}$	6.75	5.87	5.21	4.51	4.76	2.97
	%Inhibition	—	9.47	21.45	34.21	24.57	41.71
8	Rate $\times 10^{-2}$	0.52	0.46	0.28	0.29	0.26	0.26
	%Inhibition	—	11.36	39.89	41.32	39.47	55.78

metal complexes, the Zn(II) complexes with IC_{50} values of 17.61 and 17.53 $\mu\text{g}/\text{mL}$ were the most active with the lowest IC_{50} value. Additionally, the Cu(II) complex showed comparable effect with IC_{50} (19.23 and 19.37 $\mu\text{g}/\text{mL}$). The antitumor activity of the compounds follow the order

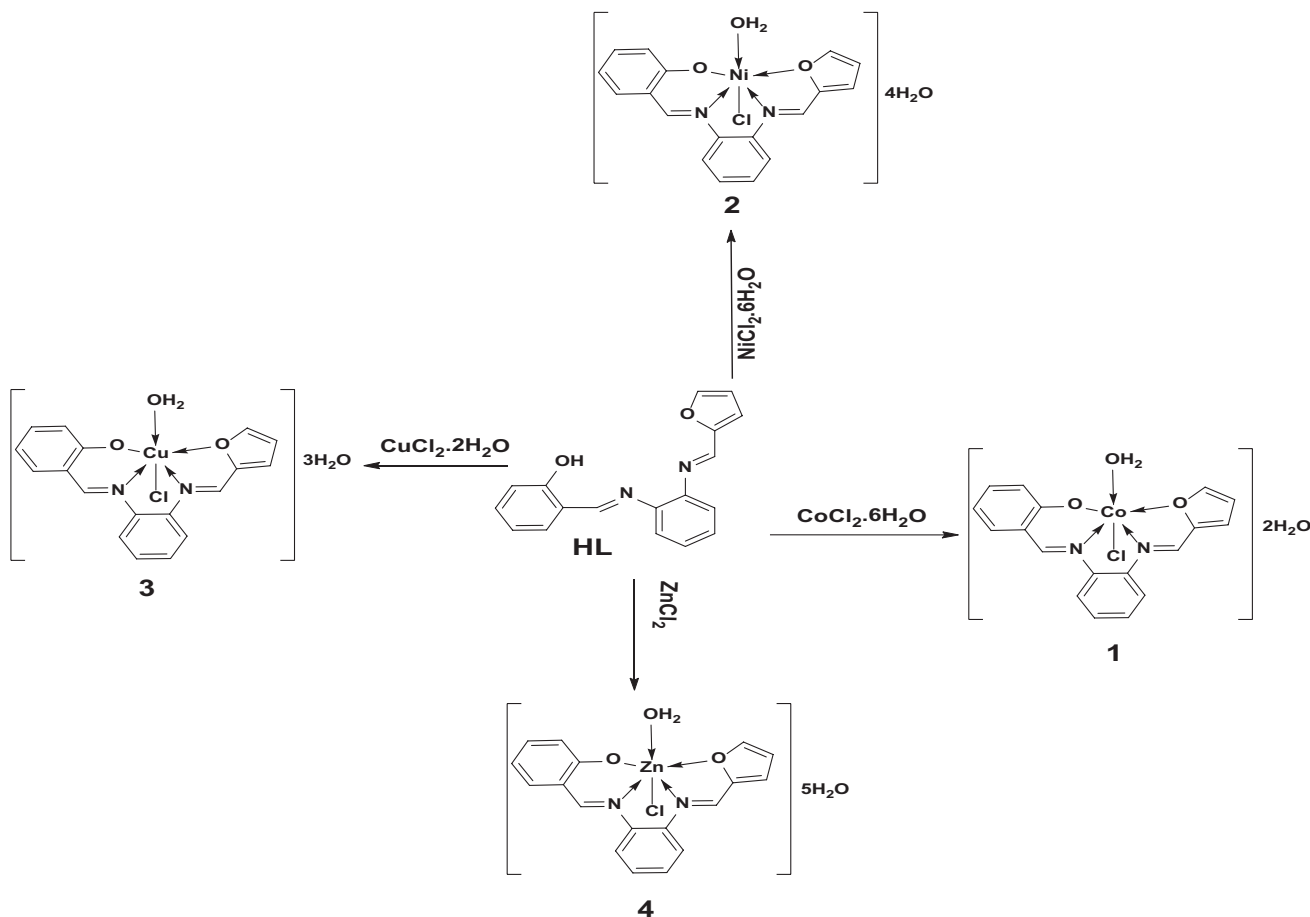
HL ligand < Co(II) complex < Cu(II) complex < Ni(II) complex < Zn(II) complex for both colon carcinoma cell (HCT-116) and mouse myelogenous leukemia carcinoma (M-NFS-60).

3.6.2 | Antimicrobial activity

The antimicrobial activity of HL ligand and its Co(II), Ni(II), Cu(II), and Ce(III) complexes was measured toward two Gram-positive bacteria species, namely *Streptococcus pneumonia* and *Bacillus subtilis*, and two Gram-negative bacteria species, namely *Salmonella typhi* and *Escherichia coli*, in addition to four fungi species (*Aspergillus fumigatus*, *Syncephalastrum racemosum*, *Geotricum candidum*, and *Candida tropicalis*) in comparison with ampicillin,

ciprofloxacin, and amphotericin B as standards. The antibacterial and antifungal activities are given in Table 12 and represented graphically in Figures S9 and S10. The following conclusions have been drawn:

1. HL and its Co(II), Ni(II), Cu(II), and Zn(II) complexes possess a broad spectrum of activity against the sensitive organisms except *Syncephalastrum racemosum* and *Salmonella typhi*, as they did not show any activity toward them. Similarly, no effect was observed for the Co(II) complex toward any sensitive organisms.
2. No effect was observed for the HL ligand toward all sensitive organisms, and such inhibition was enhanced on complexation especially in case of Ni(II), Cu(II), and Zn(II) complexes, but less than the standard used.
3. The Zn(II) complex displayed high activity toward all sensitive organisms except *Candida tropicalis* and *Salmonella typhi*.



SCHEME 1 Synthesis of the metal complexes Schiff base-derived from HL with Co(II), Ni(II), Cu(II), and Zn(II) ions

- The Ni(II) and Cu(II) complexes displayed high activity toward all sensitive organisms except *Syncephalastrum racemosum*, *Candida tropicalis*, and *Salmonella typhi*.
- The antimicrobial activity of the synthesized complexes is promising; so determining the minimum inhibitory concentration (MIC) for the synthesized complexes is recommended.

3.6.3 | Corrosion inhibition

The weight loss method for monitoring the corrosion rate is useful because of its simple application method and reliability. The presence of O and N atoms in the ligand has an inhibitory effect on steel: we find that it has inhibition of 3.84% after 2 hr and the inhibition effect increases to 9.47% and 11.36% after 4 and 8 hr, respectively. The Co(II), Ni(II), Cu(II), and Zn(II) complexes make good inhibitors on steel. These metals complexes with the HL ligand have an inhibition effect on steel, as given in Table 13 and in Figure S11. The inhibition rate follows the order

HCl < HL < Co(II) complex < Cu(II) complex < Ni(II) complex < Zn(II) complex.

The experiment was repeated after 2, 4, and 8 hr. It shows that the inhibition rate increases with increasing time in the ligand and its complexes in the following order:

HCl < HL < Co(II) complex < Cu(II) complex < Ni(II) complex < Zn(II) complex.

4 | CONCLUSIONS

The geometrical structures of the complexes of the furan-Schiff base ligand HL with Co(II), Ni(II), Cu(II), and Zn(II) ions were confirmed by the elemental analyses, IR, ^1H , ^{13}C NMR, molar conductance, magnetic moment, UV-vis, mass spectra, ESR spectra, and thermal analyses data. Thus, from the IR spectra, it was concluded that furan-Schiff base ligand HL behaves as a Schiff base tetradentate ligand with one N_2O_2 site coordinating to the metal ions via the two azomethine N groups, the furan O ring, and the deprotonated phenolic O group. From the molar conductance data of the complexes (Λ_m), it was concluded that the complexes of furan-Schiff base ligand HL can be considered non-electrolytes. The ^1H NMR spectra of the free furan-Schiff base ligand HL shows that the OH signal, which appeared in the spectrum of furan-Schiff base ligand HL at 11.93 ppm, completely disappeared in the spectra of its $[\text{ZnL}(\text{H}_2\text{O})\text{Cl}] \cdot 5\text{H}_2\text{O}$ complex, indicating that the OH proton is removed by the chelation with Zn(II) ion. The octahedral geometry of the complexes was confirmed using the DFT method from DMOL3 calculations, UV-vis, magnetic moment

measurements, ESR, ligand field, and kinetic parameters. The ligand and their metal complexes exhibited considerable antimicrobial and antitumor activities. The corrosion inhibition of steel sheets in HCl using the synthesized Schiff base and their metal complexes as inhibitors was studied using the weight loss method. The geometric structure of the complexes is shown in Scheme 1.

ACKNOWLEDGMENTS

This work was funded by the Deanship of Scientific Research at Princess Nourah bint Abdulrahman University, through the Research Groups Program Grant no. (RGP-1438-00).

REFERENCES

- [1] L. F. Lindoy, *Coord. Chem. Rev.* **1969**, *4*, 41.
- [2] P. A. Vigato, S. Tamburini, *Coord. Chem. Rev.* **2004**, *248*, 1717.
- [3] M. M. Al-Mogren, A. M. A. Alaghaz, E. A. Ebrahim, *Spectrochim. Acta Part A* **2013**, *114*, 695.
- [4] A. Dolega, *Coord. Chem. Rev.* **2010**, *254*, 916.
- [5] T. C. Harrop, P. K. Mascharak, *Acc. Chem. Res.* **2004**, *37*, 253.
- [6] H. L. Kwong, H. L. Yeung, C. T. Yeung, W. S. Lee, C. S. Lee, W. L. Wong, *Coord. Chem. Rev.* **2007**, *251*, 2188.
- [7] L. A. Saghatforoush, F. Chalabian, A. Aminkhani, G. Karimnezhad, S. Ershad, *Eur. J. Med. Chem.* **2009**, *44*, 4490.
- [8] J. T. Spence, *Coord. Chem. Rev.* **1983**, *48*, 59.
- [9] S. Gupta, A. K. Barik, S. Pal, A. Hazra, S. Roy, R. J. Butcher, S. K. Kar, *Polyhedron* **2007**, *26*, 133.
- [10] E. B. Seena, M. R. P. Kurup, *Polyhedron* **2007**, *26*, 3595.
- [11] A. A. Dehghani-Firouzabadi, F. Motevaselilyan, *Eur. J. Chem.* **2014**, *5*, 635.
- [12] A. A. Soliman, W. Linert, *Monatsh. Chem.* **2007**, *138*, 175.
- [13] S. Durmus, A. Atahan, M. Zengin, *Spectrochim. Acta Part A* **2011**, *84*, 1.
- [14] S. M. Abdallah, G. G. Mohamed, M. A. Zayed, M. S. A. El-Ela, *Spectrochim. Acta Part A* **2009**, *73*, 833.
- [15] (a) M. Ghosh, M. Layek, M. Fleck, R. Saha, D. Bandyopadhyay, *Polyhedron* **2015**, *85*, 312. (b) S. Sujarani, A. Ramu, *J. Mol. Struct.* **2015**, *1079*, 353.
- [16] R. A. Ammar, A. M. A. Alaghaz, M. E. Zayed, L. A. Al-Bedair, *J. Mol. Struct.* **2017**, *1141*, 368.
- [17] Accelrys Software Inc., Materials studio v 5.0, copyright, Accelrys Software Inc., **2009**.
- [18] W. J. Hehre, L. Radom, P. V. R. Schlyer, J. A. Pople, *Ab Initio Molecular Orbital Theory*, Wiley, New York **1986**.
- [19] A. Kessi, B. Delley, *Int. J. Quantum Chem.* **1998**, *68*, 135.
- [20] B. Hammer, L. B. Hansen, J. K. Nørskov, *Phys. Rev. B* **1999**, *59*, 7413.
- [21] A. Matveev, M. Staufner, M. Mayer, N. Rösch, *Int. J. Quantum Chem.* **1999**, *75*, 863.
- [22] B. K. Patel, S. C. Chaudhury, *J. Ind. Chem. Soc.* **1988**, *LXV*, 661.
- [23] W. J. Geary, *Coord. Chem. Rev.* **1971**, *7*, 81.
- [24] K. Nakamoto, *Infrared & Raman Spectra of Inorganic & Coordination Compounds, Part-B*, 5th ed., Wiley Interscience Publications, New York **1997**.
- [25] R. D. Salman, R. D. Farrant, J. C. Lindon, *Spectrosc. Lett.* **1991**, *24*(9), 1071.
- [26] J. Devi, N. Batra, R. Malhotra, *Spectrochim. Acta A* **2012**, *97*, 397.
- [27] E. Keskioglu, B. Güündüzalp, S. Çete, F. Hamurcu, B. Erk, *Spectrochim. Acta A* **2008**, *70*, 634.
- [28] A. M. A. Alaghaz, Y. A. Ammar, H. A. Bayoumi, S. A. Aldhlmani, *J. Mol. Struct.* **2014**, *1074*, 359.
- [29] A. M. A. Alaghaz, R. A. A. Ammar, *Eur. J. Med. Chem.* **2010**, *45*, 1314.
- [30] C. K. Jorgensen, *Acta Chim. Scand.* **1956**, *10*, 500.
- [31] A. M. A. Alaghaz, M. E. Zayed, S. A. Alharbi, R. A. A. Ammar, A. Elhenawy, *J. Mol. Struct.* **2015**, *1084*, 352.
- [32] R. Shirley, *The CRYSFIRE System for Automatic Powder Indexing: Users Manual*, Lattice Press, England **2002**.
- [33] A. W. Coats, J. P. Redfern, *Nature* **1964**, *201*, 68.
- [34] H. H. Horowitz, G. Metzger, *J. Anal. Chem.* **1963**, *35*, 1464.
- [35] G. O. Piloyan, T. D. Pyabonikar, C. S. Novikova, *Nature* **1966**, *212*, 1229.
- [36] L. T. Valaev, G. G. Gospodinov, *Thermochim. Acta* **2001**, *370*, 15.
- [37] U. El-Ayaan, I. M. Kenawy, Y. G. Abu-el-Reash, *J. Mol. Struct.* **2007**, *871*, 14.
- [38] Accelrys Inc., Accelrys Materials Studio, versions v 6.0, Accelrys Inc., **2012**.
- [39] P. Comba, T. W. Hambley, *Molecular Modeling of Inorganic Compounds*, Weinheim, VCH **1995**.
- [40] D. X. West, J. K. Swearingen, J. Valdés-Martínez, S. Hernández-Ortega, A. K. El-Sawaf, F. V. Meurs, A. Castiñeiras, I. Garcia, E. Bermejo, *Polyhedron* **1999**, *18*, 2919.
- [41] A. A. R. Despaigne, J. D. Da Silva, A. C. M. Do Carmo, F. Sives, O. E. Piro, E. E. Castellano, H. Beraldo, *Polyhedron* **2009**, *28*, 3797.
- [42] S. Sagdinc, B. Koksoy, F. Kandemirli, S. H. Bayari, *J. Mol. Struct.* **2009**, *917*, 63.

SUPPORTING INFORMATION

Additional Supporting Information may be found online in the supporting information tab for this article.

How to cite this article: Alturiqi AS, Alaghaz A-N, Zayed ME, Ammar RA. Synthesis, characterization, biological activity, and corrosion inhibition in acid medium of unsymmetrical tetradentate N₂O₂ Schiff base complexes. *J Chin Chem Soc.* 2018;1–15. <https://doi.org/10.1002/jccs.201800027>